

1-4-2006

Search for W and Z bosons in the reaction $\bar{p}p \rightarrow$ two jets + γ at $\sqrt{s} = 1.8$ TeV

Darin Acosta

University of Florida, acosta@phys.ufl.edu

Kenneth A. Bloom

University of Nebraska-Lincoln, kbloom2@unl.edu

CDF Collaboration

Follow this and additional works at: <http://digitalcommons.unl.edu/physicsbloom>

 Part of the [Physics Commons](#)

Acosta, Darin; Bloom, Kenneth A.; and Collaboration, CDF, "Search for W and Z bosons in the reaction $\bar{p}p \rightarrow$ two jets + γ at $\sqrt{s} = 1.8$ TeV" (2006). *Kenneth Bloom Publications*. 186.

<http://digitalcommons.unl.edu/physicsbloom/186>

This Article is brought to you for free and open access by the Research Papers in Physics and Astronomy at DigitalCommons@University of Nebraska - Lincoln. It has been accepted for inclusion in Kenneth Bloom Publications by an authorized administrator of DigitalCommons@University of Nebraska - Lincoln.

Search for W and Z bosons in the reaction $\bar{p}p \rightarrow$ two jets + γ at $\sqrt{s} = 1.8$ TeV

D. Acosta,¹ T. Affolder,² M. G. Albrow,³ D. Ambrose,⁴ D. Amidei,⁵ K. Anikeev,⁶ J. Antos,⁷ G. Apollinari,³ T. Arisawa,⁸
A. Artikov,⁹ W. Ashmanskas,¹⁰ F. Azfar,¹¹ P. Azzi-Bacchetta,¹² N. Bacchetta,¹² H. Bachacou,¹³ W. Badgett,³
A. Barbaro-Galtieri,¹³ V. E. Barnes,¹⁴ B. A. Barnett,¹⁵ S. Baroiant,¹⁶ M. Barone,¹⁷ G. Bauer,⁶ F. Bedeschi,¹⁸ S. Behari,¹⁵
S. Belforte,¹⁹ W. H. Bell,²⁰ G. Bellettini,¹⁸ J. Bellinger,²¹ D. Benjamin,²² A. Beretvas,³ A. Bhatti,²³ M. Binkley,³
D. Bisello,¹² M. Bishai,³ R. E. Blair,¹⁰ C. Blocker,²⁴ K. Bloom,⁵ B. Blumenfeld,¹⁵ A. Bocci,²³ A. Bodek,²⁵ G. Bolla,¹⁴
A. Bolshov,⁶ D. Bortoletto,¹⁴ J. Boudreau,²⁶ C. Bromberg,²⁷ M. Brozovic,²² E. Brubaker,¹³ J. Budagov,⁹ H. S. Budd,²⁵
K. Burkett,³ G. Busetto,¹² K. L. Byrum,¹⁰ S. Cabrera,²² M. Campbell,⁵ W. Carithers,¹³ D. Carlsmith,²¹ A. Castro,²⁸
D. Cauz,¹⁹ A. Cerri,¹³ L. Cerrito,²⁹ J. Chapman,⁵ C. Chen,⁴ Y. C. Chen,⁷ M. Chertok,¹⁶ G. Chiarelli,¹⁸ G. Chlachidze,³
F. Chlebana,³ M. L. Chu,⁷ J. Y. Chung,³⁰ W.-H. Chung,²¹ Y. S. Chung,²⁵ C. I. Ciobanu,²⁹ A. G. Clark,³¹ M. Coca,²⁵
A. Connolly,¹³ M. Convery,²³ J. Conway,³² M. Cordelli,¹⁷ J. Cranshaw,³³ R. Culbertson,³ D. Dagenhart,²⁴ S. D'Auria,²⁰
P. de Barbaro,²⁵ S. De Cecco,³⁴ S. Dell'Agnello,¹⁷ M. Dell'Orso,¹⁸ S. Demers,²⁵ L. Demortier,²³ M. Deninno,²⁸
D. De Pedis,³⁴ P. F. Derwent,³ C. Dionisi,³⁴ J. R. Dittmann,³ A. Dominguez,¹³ S. Donati,¹⁸ M. D'Onofrio,³¹ T. Dorigo,¹²
N. Eddy,²⁹ R. Erbacher,³ D. Errede,²⁹ S. Errede,²⁹ R. Eusebi,²⁵ S. Farrington,²⁰ R. G. Feild,³⁵ J. P. Fernandez,¹⁴ C. Ferretti,⁵
R. D. Field,¹⁸ I. Fiori,¹⁸ B. Flaughner,³ L. R. Flores-Castillo,²⁶ G. W. Foster,³ M. Franklin,³⁶ J. Friedman,⁶ H. Frisch,³⁷
I. Furic,⁶ M. Gallinaro,²³ M. Garcia-Sciveres,¹³ A. F. Garfinkel,¹⁴ C. Gay,³⁵ D. W. Gerdes,⁵ E. Gerstein,³⁸ S. Giagu,³⁴
P. Giannetti,¹⁸ K. Giolo,¹⁴ M. Giordani,¹⁹ P. Giromini,¹⁷ V. Glagolev,⁹ D. Glenzinski,³ M. Gold,³⁹ N. Goldschmidt,⁵
J. Goldstein,¹¹ G. Gomez,⁴⁰ M. Goncharov,⁴¹ I. Gorelov,³⁹ A. T. Goshaw,²² Y. Gotra,²⁶ K. Goulianos,²³ A. Gresele,²⁸
C. Grosso-Pilcher,³⁷ M. Guenther,¹⁴ J. Guimaraes da Costa,³⁶ C. Haber,¹³ S. R. Hahn,³ E. Halkiadakis,²⁵ R. Handler,²¹
F. Happacher,¹⁷ K. Hara,⁴² R. M. Harris,³ F. Hartmann,⁴³ K. Hatakeyama,²³ J. Hauser,⁴⁴ J. Heinrich,⁴ M. Hennecke,⁴³
M. Herndon,¹⁵ C. Hill,² A. Hocker,²⁵ K. D. Hoffman,³⁷ S. Hou,⁷ B. T. Huffman,¹¹ R. Hughes,³⁰ J. Huston,²⁷ C. Issever,²
J. Incandela,² G. Introzzi,¹⁸ M. Iori,³⁴ A. Ivanov,²⁵ Y. Iwata,⁴⁵ B. Iyutin,⁶ E. James,³ M. Jones,¹⁴ T. Kamon,⁴¹ J. Kang,⁵
M. Karagoz Unel,⁴⁶ S. Kartal,³ H. Kasha,³⁵ Y. Kato,⁴⁷ R. D. Kennedy,³ R. Kephart,³ B. Kilminster,²⁵ D. H. Kim,⁴⁸
H. S. Kim,²⁹ M. J. Kim,³⁸ S. B. Kim,⁴⁸ S. H. Kim,⁴² T. H. Kim,⁶ Y. K. Kim,³⁷ M. Kirby,²² L. Kirsch,²⁴ S. Klimentenko,¹
P. Koehn,³⁰ K. Kondo,⁸ J. Konigsberg,¹ A. Korn,⁶ A. Korytov,¹ J. Kroll,⁴ M. Kruse,²² V. Krutelyov,⁴¹ S. E. Kuhlmann,¹⁰
N. Kuznetsova,³ A. T. Laasanen,¹⁴ S. Lami,²³ S. Lammel,³ J. Lancaster,²² K. Lannon,³⁰ M. Lancaster,⁴⁹ R. Lander,¹⁶
A. Lath,³² G. Latino,³⁹ T. LeCompte,¹⁰ Y. Le,¹⁵ J. Lee,²⁵ S. W. Lee,⁴¹ N. Leonardo,⁶ S. Leone,¹⁸ J. D. Lewis,³ K. Li,³⁵
C. S. Lin,³ M. Lindgren,⁴⁴ T. M. Liss,²⁹ T. Liu,³ D. O. Litvintsev,³ N. S. Lockyer,⁴ A. Loginov,⁵⁰ M. Loreti,¹²
D. Lucchesi,¹² P. Lukens,³ L. Lyons,¹¹ J. Lys,¹³ R. Madrak,³⁶ K. Maeshima,³ P. Maksimovic,¹⁵ L. Malferrari,²⁸
M. Mangano,¹⁸ G. Manca,¹¹ M. Mariotti,¹² M. Martin,¹⁵ A. Martin,³⁵ V. Martin,⁴⁶ M. Martínez,³ P. Mazzanti,²⁸
K. S. McFarland,²⁵ P. McIntyre,⁴¹ M. Menguzzato,¹² A. Menzione,¹⁸ P. Merkel,³ C. Mesropian,²³ A. Meyer,³ T. Miao,³
R. Miller,²⁷ J. S. Miller,⁵ S. Miscetti,¹⁷ G. Mitselmakher,¹ N. Moggi,²⁸ R. Moore,³ T. Moulik,¹⁴ M. Mulhearn,⁶
A. Mukherjee,³ T. Muller,⁴³ A. Munar,⁴ P. Murat,³ J. Nachtman,³ S. Nahn,³⁵ I. Nakano,⁴⁵ R. Napora,¹⁵ F. Niell,⁵
C. Nelson,³ T. Nelson,³ C. Neu,³⁰ M. S. Neubauer,⁶ C. Newman-Holmes,³ T. Nigmanov,²⁶ L. Nodulman,¹⁰ S. H. Oh,²²
Y. D. Oh,⁴⁸ T. Ohsugi,⁴⁵ T. Okusawa,⁴⁷ W. Orejudos,¹³ C. Pagliarone,¹⁸ F. Palmonari,¹⁸ R. Paoletti,¹⁸ V. Papadimitriou,³³
J. Patrick,³ G. Pauletta,¹⁹ M. Paulini,³⁸ T. Pauly,¹¹ C. Paus,⁶ D. Pellett,¹⁶ A. Penzo,¹⁹ T. J. Phillips,²² G. Piacentino,¹⁸
J. Piedra,⁴⁰ K. T. Pitts,²⁹ A. Pompoš,¹⁴ L. Pondrom,²¹ G. Pope,²⁶ T. Pratt,¹¹ F. Prokoshin,⁹ J. Proudfoot,¹⁰ F. Ptohos,¹⁷
O. Poukhov,⁹ G. Punzi,¹⁸ J. Rademacker,¹¹ A. Rakitine,⁶ F. Ratnikov,³² H. Ray,⁵ A. Reichold,¹¹ P. Renton,¹¹
M. Rescigno,³⁴ F. Rimondi,²⁸ L. Ristori,¹⁸ W. J. Robertson,²² T. Rodrigo,⁴⁰ S. Rolli,⁵¹ L. Rosenson,⁶ R. Roser,³
R. Rossin,¹² C. Rott,¹⁴ A. Roy,¹⁴ A. Ruiz,⁴⁰ D. Ryan,⁵¹ A. Safonov,¹⁶ R. St. Denis,²⁰ W. K. Sakumoto,²⁵ D. Saltzberg,⁴⁴
C. Sanchez,³⁰ A. Sansoni,¹⁷ L. Santi,¹⁹ S. Sarkar,³⁴ P. Savard,⁵² A. Savoy-Navarro,³ P. Schlabach,³ E. E. Schmidt,³
M. P. Schmidt,³⁵ M. Schmitt,⁴⁶ L. Scodellaro,¹² A. Scribano,¹⁸ A. Sedov,¹⁴ S. Seidel,³⁹ Y. Seiya,⁴² A. Semenov,⁹
F. Semeria,²⁸ M. D. Shapiro,¹³ P. F. Shepard,²⁶ T. Shibayama,⁴² M. Shimojima,⁴² M. Shochet,³⁷ A. Sidoti,¹² A. Sill,³³
P. Sinervo,⁵² A. J. Slaughter,³⁵ K. Sliwa,⁵¹ F. D. Snider,³ R. Snihur,⁴⁹ M. Spezziga,³³ F. Spinella,¹⁸ M. Spiropulu,²
L. Spiegel,³ A. Stefanini,¹⁸ J. Strologas,³⁹ D. Stuart,² A. Sukhanov,¹ K. Sumorok,⁶ T. Suzuki,⁴² R. Takashima,⁴⁵
K. Takikawa,⁴² M. Tanaka,¹⁰ M. Tecchio,⁵ R. J. Tesarek,³ P. K. Teng,⁷ K. Terashi,²³ S. Tether,⁶ J. Thom,³
A. S. Thompson,²⁰ E. Thomson,³⁰ P. Tipton,²⁵ S. Tkaczyk,³ D. Toback,⁴¹ K. Tollefson,²⁷ D. Tonelli,¹⁸ M. Tönnesmann,²⁷
H. Toyoda,⁴⁷ W. Trischuk,⁵² J. Tseng,⁶ D. Tsybychev,¹ N. Turini,¹⁸ F. Ukegawa,⁴² T. Unverhau,²⁰ T. Vaiciulis,²⁵
A. Varganov,⁵ E. Vataga,¹⁸ S. Vejcik III,³ G. Velev,³ G. Veramendi,¹³ R. Vidal,³ I. Vila,⁴⁰ R. Vilar,⁴⁰ I. Volobouev,¹³
M. von der Mey,⁴⁴ R. G. Wagner,¹⁰ R. L. Wagner,³ W. Wagner,⁴³ Z. Wan,³² C. Wang,²² M. J. Wang,⁷ S. M. Wang,¹

B. Ward,²⁰ S. Waschke,²⁰ D. Waters,⁴⁹ T. Watts,³² M. Weber,¹³ W. C. Wester III,³ B. Whitehouse,⁵¹ A. B. Wicklund,¹⁰ E. Wicklund,³ H. H. Williams,⁴ P. Wilson,³ B. L. Winer,³⁰ S. Wolbers,³ M. Wolter,⁵¹ S. Worm,³² X. Wu,³¹ F. Würthwein,⁶ U. K. Yang,³⁷ W. Yao,¹³ G. P. Yeh,³ K. Yi,¹⁵ J. Yoh,³ T. Yoshida,⁴⁷ I. Yu,⁴⁸ S. Yu,⁴ J. C. Yun,³ L. Zanello,³⁴ A. Zanetti,¹⁹ F. Zetti,¹³ and S. Zucchelli¹³

(CDF Collaboration)

- ¹University of Florida, Gainesville, Florida 32611, USA
²University of California at Santa Barbara, Santa Barbara, California 93106, USA
³Fermi National Accelerator Laboratory, Batavia, Illinois 60510, USA
⁴University of Pennsylvania, Philadelphia, Pennsylvania 19104, USA
⁵University of Michigan, Ann Arbor, Michigan 48109, USA
⁶Massachusetts Institute of Technology, Cambridge, Massachusetts 02139, USA
⁷Institute of Physics, Academia Sinica, Taipei, Taiwan 11529, Republic of China
⁸Waseda University, Tokyo 169, Japan
⁹Joint Institute for Nuclear Research, RU-141980 Dubna, Russia
¹⁰Argonne National Laboratory, Argonne, Illinois 60439, USA
¹¹University of Oxford, Oxford OX1 3RH, United Kingdom
¹²Istituto Nazionale di Fisica Nucleare, Università di Padova, Sezione di Padova, I-35131 Padova, Italy
¹³Ernest Orlando Lawrence Berkeley National Laboratory, Berkeley, California 94720, USA
¹⁴Purdue University, West Lafayette, Indiana 47907, USA
¹⁵The Johns Hopkins University, Baltimore, Maryland 21218, USA
¹⁶University of California at Davis, Davis, California 95616, USA
¹⁷Laboratori Nazionali di Frascati, Istituto Nazionale di Fisica Nucleare, I-00044 Frascati, Italy
¹⁸Istituto Nazionale di Fisica Nucleare, University and Scuola Normale Superiore of Pisa, I-56100 Pisa, Italy
¹⁹Istituto Nazionale di Fisica Nucleare, University of Trieste, I-34127 Trieste, Italy
²⁰Glasgow University, Glasgow G12 8QQ, United Kingdom
²¹University of Wisconsin, Madison, Wisconsin 53706, USA
²²Duke University, Durham, North Carolina 27708, USA
²³Rockefeller University, New York, New York 10021, USA
²⁴Brandeis University, Waltham, Massachusetts 02254, USA
²⁵University of Rochester, Rochester, New York 14627, USA
²⁶University of Pittsburgh, Pittsburgh, Pennsylvania 15260, USA
²⁷Michigan State University, East Lansing, Michigan 48824, USA
²⁸Istituto Nazionale di Fisica Nucleare, University of Bologna, I-40127 Bologna, Italy
²⁹University of Illinois, Urbana, Illinois 61801, USA
³⁰The Ohio State University, Columbus, Ohio 43210, USA
³¹University of Geneva, CH-1211 Geneva 4, Switzerland
³²Rutgers University, Piscataway, New Jersey 08855, USA
³³Texas Tech University, Lubbock, Texas 79409, USA
³⁴Istituto Nazionale de Fisica Nucleare, Sezione di Roma, University di Roma I, "La Sapienza," I-00185 Roma, Italy
³⁵Yale University, New Haven, Connecticut 06520, USA
³⁶Harvard University, Cambridge, Massachusetts 02138, USA
³⁷Enrico Fermi Institute, University of Chicago, Chicago, Illinois 60637, USA
³⁸Carnegie Mellon University, Pittsburgh, Pennsylvania 15213, USA
³⁹University of New Mexico, Albuquerque, New Mexico 87131, USA
⁴⁰Instituto de Fisica de Cantabria, CSIC-University of Cantabria, 39005 Santander, Spain
⁴¹Texas A&M University, College Station, Texas 77843, USA
⁴²University of Tsukuba, Tsukuba, Ibaraki 305, Japan
⁴³Institut für Experimentelle Kernphysik, Universität Karlsruhe, 76128 Karlsruhe, Germany
⁴⁴University of California at Los Angeles, Los Angeles, California 90024, USA
⁴⁵Hiroshima University, Higashi-Hiroshima 724, Japan
⁴⁶Northwestern University, Evanston, Illinois 60208, USA
⁴⁷Osaka City University, Osaka 588, Japan
⁴⁸Center for High Energy Physics, Kyungpook National University, Taegu 702-701, Korea, Seoul National University, Seoul 151-742, Korea, and SungKyunKwan University, Suwon 440-746, Korea
⁴⁹University College London, London WC1E 6BT, United Kingdom
⁵⁰Institution for Theoretical and Experimental Physics, ITEP, Moscow 117259, Russia

⁵¹*Tufts University, Medford, Massachusetts 02155, USA*⁵²*Institute of Particle Physics, University of Toronto, Toronto, Canada M5S 1A7*

(Received 13 July 2005; published 6 January 2006)

We present a study of the dijet invariant mass distribution for the reaction $\bar{p}p \rightarrow$ two jets + γ + X , at a center of mass energy of 1.8 TeV, using data collected by the CDF experiment. We compare the data to predictions for the production of a photon with two jets, together with the resonant processes $\bar{p}p \rightarrow W/Z + \gamma + X$, in which the W and Z bosons decay hadronically. A fit is made to the dijet invariant mass distribution combining the nonresonant background and resonant processes. We use the result to establish a limit for the inclusive production cross section of $W/Z + \gamma$ with hadronic decay of the W and Z bosons.

DOI: [10.1103/PhysRevD.73.012001](https://doi.org/10.1103/PhysRevD.73.012001)

PACS numbers: 13.85.Qk, 13.38.Dg, 13.87.Fh

I. INTRODUCTION

The production of final states containing W or Z bosons in association with a photon (γ) in $\bar{p}p$ collisions at $\sqrt{s} = 1.8$ TeV has been studied by the CDF and D0 Collaborations using event samples in which the W and Z bosons decay to leptons [1]. Identification of $W\gamma$ and $Z\gamma$ events in which the W/Z decay hadronically is experimentally difficult because of a large background from direct production of two-jet + γ and three-jet events. A study of the general kinematic characteristics of two-jet + γ production has been conducted using 16 pb^{-1} of data from CDF run 1a, however the dijet invariant mass distribution was not investigated [2].

We present a search for evidence of $\gamma + W/Z \rightarrow q\bar{q}$ final states in 90 pb^{-1} of $\bar{p}p$ data. The data were collected with the CDF detector during run 1b of the Tevatron. A search for two-jet + γ events was conducted within the data subset in which a photon candidate had electromagnetic transverse energy greater than 23 GeV. The dijet invariant mass distribution was fit to a mixture of boson resonance decay and QCD background.

The methods established in this analysis [3] could prove useful for identifying similar signals coming from $X \rightarrow jj$ decay which are embedded in large QCD background.

II. THE DETECTOR

A comprehensive description of the Collider Detector at Fermilab (CDF) may be found in [4]. We used a coordinate system with z along the proton beam, azimuthal angle ϕ , polar angle θ , and pseudorapidity $\eta = -\ln \tan(\theta/2)$. The transverse energy of a particle (e.g. photon, electron, jet) was defined as $E_T = E \sin\theta$. The primary components relevant to this analysis were those that measure jet energies and positions, photon energies, positions and profiles, and those that establish the $\bar{p}p$ interaction vertex.

The central tracking chamber (CTC) and vertex tracking chamber (VTX) were used to measure momenta and directions of the charged tracks associated with jets. The tracking chambers were located within 1.4 T axial magnetic field. The CTC was a drift chamber which provides space point information used to construct the trajectories of charged particles. It covered a rapidity range of $|\eta| < 1.1$. The VTX was a time projection chamber positioned

between the beam pipe and the CTC that provided an improved interaction vertex measurement with the extrapolation of tracks reconstructed in the CTC.

Scintillator-based electromagnetic (CEM) and hadronic (CHA) calorimeters in the central region ($|\eta| \leq 1.1$) were arranged in projective towers of size $\Delta\eta \times \Delta\phi \approx 0.1 \times 0.26$. The end-wall hadronic calorimeter and the end-plug electromagnetic and hadronic calorimeters extended the rapidity coverage out to $|\eta| \leq 2.4$.

Two additional detector elements were used for photon identification. The central strip chambers (CES) were multiwire proportional chambers with segmented cathode strips. The CES was positioned near the shower maximum of the central electromagnetic detector. The anode wires measured ϕ and the cathode strips measured η for showers in the CEM. The central preradiator (CPR) was a set of multiwire proportional chambers, positioned between the magnet solenoid and the CEM. It was used to measure the electromagnetic shower pulse heights of electron-positron pairs from photons converting in a solenoid of thickness 1.1 radiation lengths. The CES and the CPR detector systems provided discrimination between single photons and multiphoton showers arising from π^0 and η decays.

III. EVENT SELECTION

Events with photon candidates were selected using a trigger which required a high threshold of energy deposited in the central electromagnetic calorimeter. Photon clusters were reconstructed by combining the energy from neighboring CEM cells with a seed cell having energy above a threshold of 3 GeV. A photon candidate was required to have clustered energy $E_T > 23$ GeV.

The trigger acceptance for photon candidates has been measured as a function of the photon transverse momentum [5]. The acceptance plateaus for the photons with $E_T \geq 30$ GeV at 0.970 ± 0.006 .

In the offline data analysis, the measured photon energies were corrected using an algorithm taking into account variations of CEM response within a cell, cell-to-cell energy sharing, and a global transverse energy scale [6]. A photon candidate was required to be isolated, with less than 15% additional energy ($E_{\text{CEM}} + E_{\text{CHA}}$) within a cone of radius $\Delta R = \sqrt{\Delta\phi^2 + \Delta\eta^2} < 0.4$ centered on the photon

direction. In order to reject electrons, a tracking isolation requirement was imposed by summing the transverse momentum of tracks within the $\Delta R < 0.4$ cone around the photon direction. The sum of p_T of the tracks was required to be less than $2 \text{ GeV}/c$.

The ratio of the energy deposited in the hadronic calorimeter (E_{HAD}) to the energy deposited in the electromagnetic calorimeter (E_{CEM}) for a photon candidate passing the above cuts must satisfy the requirement

$$\frac{E_{\text{HAD}}}{E_{\text{CEM}}} \leq 0.055 + 0.00045E(\gamma),$$

with $E(\gamma)$ in GeV. Typically, for a photon, the above ratio is less than 10%. A lateral sharing parameter for CEM clusters measures the spread of energy over calorimeter cells adjacent to the seed cell and selects photons based upon the spread expected from measurements in an electron test beam.

The photons had to pass fiducial cuts that require sufficient shower containment in the CES chambers. The highest energy strip cluster and the highest energy wire cluster were chosen to estimate the position and transverse profile of a photon candidate. Any additional clusters in the CES within the boundaries of the calorimeter energy cluster had to have energy less than $2.39 + 0.01E_T(\gamma) \text{ GeV}$.

Multiphoton backgrounds from π^0 and η decays are suppressed by requiring the transverse profile of the shower energy observed in the CES to match to a reference profile measured using an electron test beam. A partial separation of direct photons from multiphoton backgrounds was made based on the quality of the shower shape agreement. Additional details of the photon cuts may be found in [7].

The energy from identified photons is removed from the calorimeter cells and the remaining energy is clustered to reconstruct jets. Hadronic jets are identified using a cone clustering algorithm [8]. The energies of jets clustered with a cone size of $\Delta R < 0.7$ were corrected for calorimeter nonlinearity and cell-to-cell nonuniformity. A correction takes into account energy deposition from particles not associated with the parent parton falling within the jet clustering cone, and an out-of-cone correction for the underlying event accounts for energy from the jet which is radiated outside the jet clustering cone.

The sample of events with exactly two jets having E_T greater than 15 GeV and $|\eta| \leq 1.1$ is used. The restricted rapidity range insures that the reconstruction efficiency for tracks associated with these jets is uniform. Any additional jets present in the event within $|\eta| < 2.4$ must have $E_T \leq 10 \text{ GeV}$. Each of the two central jets must include at least one well-reconstructed track, which is used to calculate the vertex position. The vertices determined from the tracking information from the two jets in an event must lie within 10 cm of each other. This cut removes instances of jets from different $p\bar{p}$ collisions during the same beam crossing. The interaction vertex is taken to be the average of the

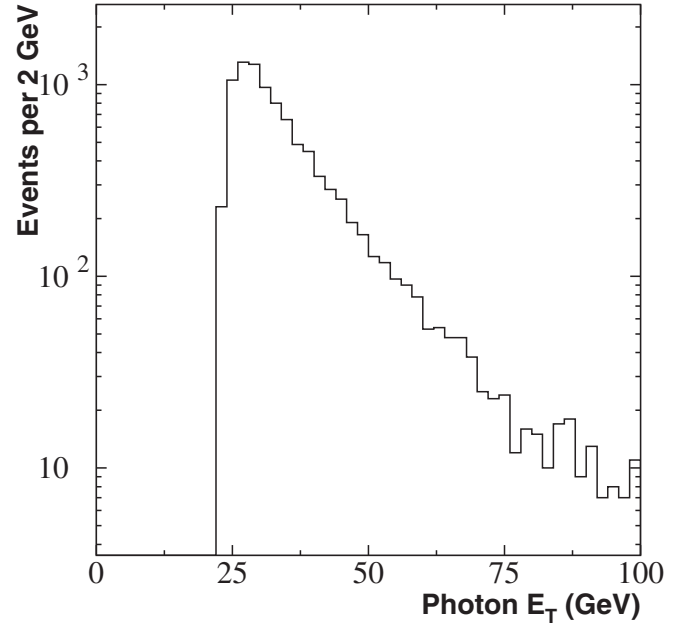


FIG. 1. Photon E_T distribution from $\gamma + \text{two-jet}$ events.

two-jet vertices and must lie within 60 cm of the center of the detector. This vertex, together with the information from the CES, is used to define the photon trajectory.

A total of approximately 2.7×10^6 triggered events was recorded. A sample of 9493 events satisfied all photon and jet selection criteria. The photon E_T distribution is shown in Fig. 1. Figure 2 shows the E_T and η distributions for the two leading jets in the event, ordered by E_T . The first jet has an average E_T of 39 GeV, while the second jet has an average E_T of 23 GeV. A plot of the dijet invariant mass

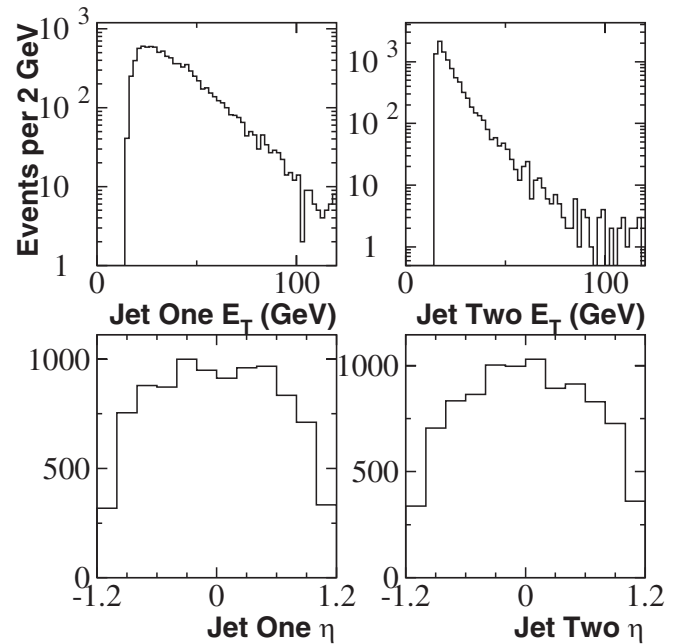


FIG. 2. The E_T and η distributions for the two leading jets.

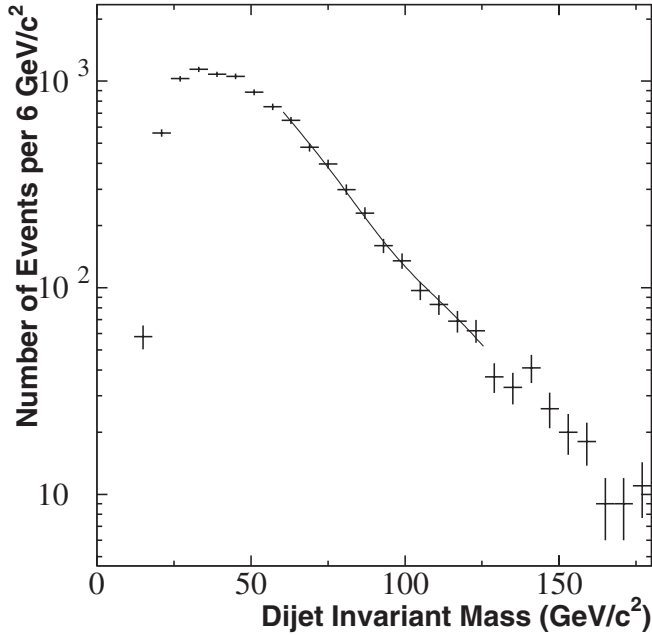


FIG. 3. Dijet mass spectrum from two-jet + γ data. There are 2656 events in the m_{jj} region from 60 to 126 GeV/c^2 . The solid fit corresponds to the background + signal fit as described in Sec. VI.

distribution is shown in Fig. 3. The dijet invariant mass m_{jj} is defined as $\sqrt{(E_1 + E_2)^2 - (\vec{P}_1 + \vec{P}_2)^2}$, where E_i and \vec{P}_i are the energies and momenta of the two leading jets.

IV. EVENT GENERATION AND SIMULATION

There are several physical processes which produce the two-jet + photon final state. Our primary goal is the study of resonant $W/Z + \gamma$ production with W/Z decaying to jets. In addition to these signal events, we also generate two QCD backgrounds which contribute to the two-jet + photon events. The first contributor is nonresonant two-jet + photon production and the second is three-jet production where one of the jets is misidentified as a photon.

A CDF detector simulation produces event records with the same structure as the data. These generated events are then subject to the same photon and jet selection cuts, and detector geometric acceptance, as applied to the data.

A. Signal simulation

The signal processes $\bar{p}p \rightarrow W + \gamma$ and $\bar{p}p \rightarrow Z + \gamma$, in which the W/Z decay to two jets, are modeled using a leading order (LO) matrix element calculation [9] which includes contributions from initial and final state inner bremsstrahlung processes. The Monte Carlo simulation produces photons with $E_T \geq 15$ GeV and ΔR between the photon and partons greater than 0.4. We also require that the invariant mass of the quark-antiquark pair from the W/Z decay is greater than the boson mass minus 3 times

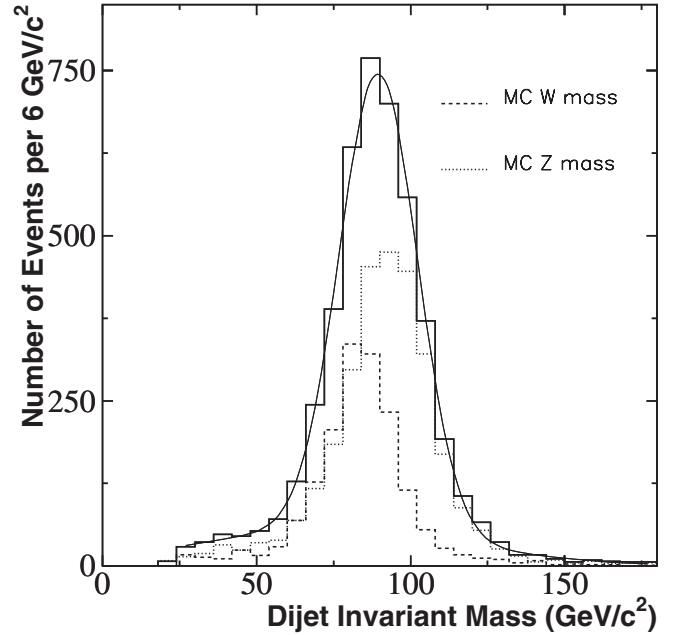


FIG. 4. The invariant mass distributions of the two leading jets from the LO $W\gamma$ and $Z\gamma$ simulations, together with their sum (solid line). The combined invariant mass was fit with a double Gaussian as described in Sec. V.

the boson natural width ($\sqrt{\hat{s}} > M_V - 3\Gamma_V$). This latter cut tends to suppress final state bremsstrahlung and produces a characteristic W/Z resonant mass peak that simulates the signal searched for in our data (see Sec. VI). The factorization scale was set equal to the square of the colliding partons center of mass energy $\sqrt{\hat{s}}$. The MRSA' parton distribution functions were used. The parton-level events are run through HERWIG for parton shower evolution and hadronization [10]. The resulting dijet mass distributions from W and Z decays, together with the combined distribution, are shown in Fig. 4.

The $W\gamma$ and $Z\gamma$ signal acceptance is calculated with a full CDF detector simulation. The details of the acceptance calculations are presented in Tables I and II for the $W\gamma$ and $Z\gamma$ events, respectively. The uncertainty in the acceptances for each cut were estimated by varying the upper and lower limits on the cut parameters and measuring the effects on

TABLE I. $W\gamma$ event selection acceptances.

$W\gamma$ sample	Events	%	Error %
Generated	97 298	100	
Photon $ \eta $	55 487	57.03	+2.40, -2.83
Photon ID	25 939	26.67	+1.13, -2.02
Photon trigger	9 567	9.83	+0.62, -0.83
Jet $E_T + \eta $	1 691	1.74	+0.30, -0.29
Extra jet	1 691	1.74	+0.31, -0.30
Tracks	1 677	1.72	+0.31, -0.30

TABLE II. $Z\gamma$ event selection acceptances.

$Z\gamma$ sample	Events	%	Error %
Generated	102 210	100	
Photon $ \eta $	68 563	67.08	+2.55, -3.16
Photon ID	37 080	36.28	+1.38, -2.78
Photon trigger	15 294	14.96	+0.86, -1.45
Jet $E_T + \eta $	2 959	2.90	+0.47, -0.49
Extra jet	2 959	2.90	+0.48, -0.51
Tracks	2 946	2.88	+0.48, -0.51

the number of events passing the cuts. The errors in the Tables I and II represent cumulative errors on the acceptance, where all the errors of the subsequent cuts are added in quadrature.

The photon η cut was varied from 1.0 to 1.2. The photon identification (photon ID) combines effects of the three consecutive cuts. This selection allowed a photon candidate to have up to one charged 3D CTC track as long as the sum of the transverse momentum of the tracks with $\Delta R < 0.4$ of the photon direction stayed less than $2 \text{ GeV}/c$. In addition, the isolation of a photon candidate was ensured by the cut on additional energy ($E_{\text{CEM}} + E_{\text{CHA}} < 15\%$) within a cone $\Delta R < 0.4$. To understand how the photon ID effects the selection, the number of charged tracks allowed in a photon cluster cone was varied from zero to two. The effect of this change was propagated through to the photon isolation cuts, and the resulting variation in the acceptance was used as an estimate of the systematic uncertainty in the photon identification. Finally, we estimated the uncertainty in the acceptance due to the photon trigger. The key threshold points in the turn-on function [5] were varied by $\pm 5\%$ from the nominal value. For example, the photons with $23 \leq E_T < 26 \text{ GeV}$ originally had 22% probability to pass the trigger. The high acceptance cut lowers this probability to 17%, while the low acceptance cut raises this probability to 27%. In addition, the photons with $26 \leq E_T < 30 \text{ GeV}$ had 77% probability to pass the trigger. Finally, photons with $E_T \geq 30 \text{ GeV}$ were passing the trigger with 97% probability. The resulting effect on the acceptance was taken as a systematic uncertainty. Tables I and II summarize the photon selection acceptances and their uncertainties.

The systematic uncertainties due to jet selection criteria can be divided into three categories: those based upon the cuts used to select the two high E_T jets ($E_T > 15 \text{ GeV}$, and $|\eta| < 1.1$); those caused by rejection of events having additional low E_T jets (additional jet cannot have $E_T > 10 \text{ GeV}$ if within $|\eta| < 2.4$); and those due to the use of charged tracks in the jets to define the event vertex. The uncertainty caused by the high E_T jet selection was estimated by varying the E_T cut from 14 to 16 GeV and the $|\eta|$ cut from 1.0 to 1.2 (see “jet E_T and η ” rows in Tables I and II). The effect of the rejection of additional jets was evaluated by varying E_T from 9.5 to 10.5 GeV and $|\eta|$ from 2.3

to 2.4 (“extra jet” rows in Tables I and II). The final uncertainty on the jet selection comes from the use of charged tracks to determine the event vertex. The upper number on the tracking uncertainty was estimated by demanding that each of the jets has at least 2 charged tracks which in addition have a very small distance from the calculated jet vertex. Variations in the track selection criteria cause almost negligible uncertainty of event acceptance shown in the last rows of Tables I and II. The final overall event selection acceptance for $W\gamma$ events is 0.017 ± 0.003 and for $Z\gamma$ events 0.029 ± 0.005 .

B. Background simulation

We use a tree level calculation for the $\gamma + \text{two-jet}$ background process which includes both prompt photon and bremsstrahlung contributions [11], followed by HERWIG for parton evolution and fragmentation. In addition, three-jet events are generated using PYTHIA [12], with JETSET performing the parton evolution and fragmentation. Each of the three leading jets was tested for misidentification as photons. This procedure was based on the probability distribution measured from jet data which describes how often a jet with a particular E_T is misidentified as a photon. The data show that a jet with $E_T \geq 23 \text{ GeV}$ has a maximum probability of 8×10^{-4} to fake a photon.

The dijet mass distribution from the data favors a background mixture of 60% two-jet + photon and 40% three-jet in which one jet fakes a photon. Figure 5 shows the dijet mass distribution for this combination of backgrounds. For

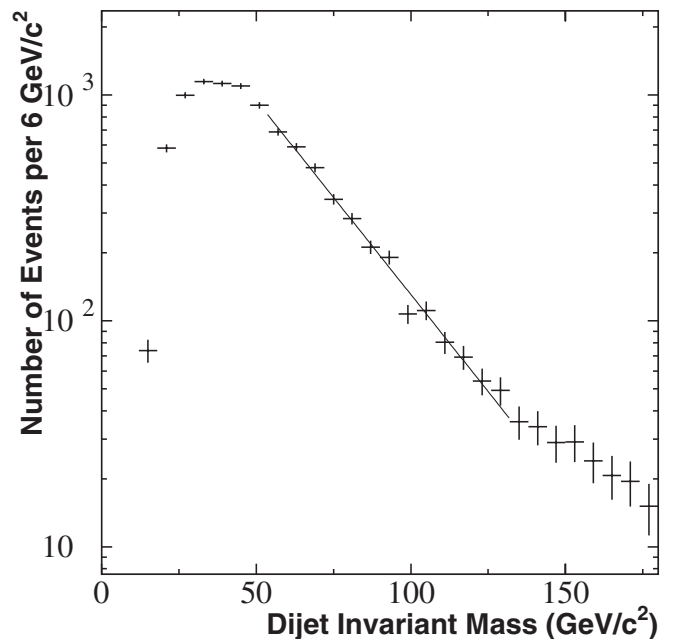


FIG. 5. Combined background of two-jet + γ events and three-jet events in which one jet is identified as a photon. The distributions are mixed in the ratio 60% to 40%. The exponential fit is presented with a solid line.

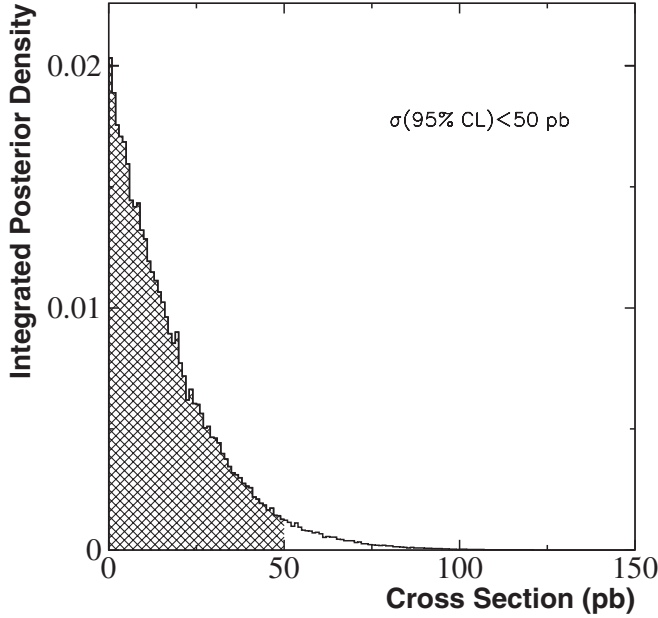


FIG. 6. Posterior density (likelihood function multiplied by Gaussian priors for \mathcal{L} and $\epsilon_{W/Z\gamma}$) integrated over \mathcal{L} and $\epsilon_{W/Z\gamma}$, versus σ .

masses between $60 \text{ GeV}/c^2$ and $126 \text{ GeV}/c^2$ the background distribution is fit well to the form $dN/dm_{jj} = A \exp(-bm_{jj})$ as shown by the solid line in Fig. 5. This slope is known to be effected by the inclusion of higher-order QCD contributions, so we leave the exponential slope of the background as a free parameter in the fit to the experimental dijet mass spectrum to a combination of signal plus background (see Sec. VI for details).

V. STANDARD MODEL PREDICTIONS FOR $W\gamma, Z\gamma$ CROSS SECTIONS

Four parton-level event samples were generated using the procedure described in Sec. IVA: $W^+ \gamma$ (where $W^+ \rightarrow u\bar{d}$), $W^- \gamma$ (where $W^- \rightarrow d\bar{u}$), $Z\gamma$ (where $Z \rightarrow u\bar{u}$), and $Z\gamma$ (where $Z \rightarrow d\bar{d}$). Partons are treated as massless in the model. In order to include the W/Z decays to heavy quarks, the initial “light” cross sections are multiplied by appropriate factors. For example, $W^+ \rightarrow u\bar{d}$ is multiplied by 2.1 to account for $c\bar{s}$, $c\bar{d}$, $u\bar{s}$, and $c\bar{b}$ decays. The same is valid for the $W^- \rightarrow d\bar{u}$. The cross section for $Z \rightarrow u\bar{u}$ is multiplied by 2.0 to account for $Z \rightarrow c\bar{c}$, while the cross section for $Z \rightarrow d\bar{d}$ is multiplied by factor 3.0 to include $Z \rightarrow s\bar{s}$, $b\bar{b}$ decays. In addition, the final cross sections are multiplied by a factor of 1.3 [13] to take into account higher-order QCD corrections.

The resulting cross section for $p\bar{p} \rightarrow W^\pm + \gamma$ with W^\pm decay to quark-antiquark is 6.35 pb , and for $p\bar{p} \rightarrow Z + \gamma$ with the Z decay to quark-antiquark is 6.52 pb . These values pertain to events generated with $E_T(\gamma) \geq 15 \text{ GeV}$, ΔR between the photon and each of the quarks $\Delta R(\gamma -$

$q) > 0.4$ and the quark-antiquark mass greater than the boson mass minus 3 times the boson natural width.

With an integrated luminosity of 90 pb^{-1} we would expect $N_{W\gamma} = 90 \times 6.35 \times 0.017 = 10^{+2}_{-2}$ events, and $N_{Z\gamma} = 90 \times 6.52 \times 0.029 = 17^{+3}_{-3}$ events. The total is 27^{+5}_{-5} events in the two-jet + photon data sample in the dijet invariant mass region between 60 and $126 \text{ GeV}/c^2$. The errors on the total number of events were added directly, as they result from the same detector systematics in the Monte Carlo simulation. The generated $W^\pm \gamma$ and $Z\gamma$ events are combined in proportion to their cross sections.

The dijet mass distribution from the combined $W/Z\gamma$ generated events shown in Fig. 4 is normalized to a total area of one and fit to a double Gaussian

$$\frac{1}{N} \frac{dN}{dm_{jj}} = S(m_{jj}),$$

$$S(m_{jj}) = S_1 e^{-(m_{jj}-m_1)^2/(2\sigma_1)^2} + S_2 e^{-(m_{jj}-m_2)^2/(2\sigma_2)^2}.$$

The fit parameters are $S_1 = 0.028 (\text{GeV}/c^2)^{-1}$, $m_1 = 89.6 \text{ GeV}/c^2$, $\sigma_1 = 12.5 \text{ GeV}/c^2$, and $S_2 = 0.002 (\text{GeV}/c^2)^{-1}$, $m_2 = 76.3 \text{ GeV}/c^2$, $\sigma_2 = 41 \text{ GeV}/c^2$. These parameters are used in fitting the dijet mass distribution from the data to a combination of an exponential background and the signal distributions.

The widths of the invariant mass spectra for simulation of W and Z production shown in Fig. 4 are consistent with the inferred mass resolution from a study of inclusive two-jet production at CDF [14]. Over the dijet mass range from 60 to $126 \text{ GeV}/c^2$ the fractional dijet mass resolution ($\delta_{m_{jj}}/m_{jj}$) is essentially constant at 15%.

VI. FITTING STANDARD MODEL PREDICTIONS TO THE DATA

A sum of predicted background and resonant dijet mass distributions is fit to a histogram of the data in 11 bins over the mass range 60 to $126 \text{ GeV}/c^2$. The fitting procedure maximizes the likelihood function:

$$L = \exp(-\chi^2/2),$$

where the χ^2 is given by

$$\chi^2(\tilde{f}, \tilde{b}) = \sum_{i=1}^n \frac{(N_i - \tilde{N}_i(\tilde{f}, \tilde{b}))^2}{\sigma_i^2}.$$

The optimal set of the two free parameters (\tilde{f}, \tilde{b}) is found by minimizing the χ^2 of the fit to the dijet mass distribution of the data. N_i and σ_i are the number of events in the i th mass bin of the data, and the statistical error. The total number of events in the mass range from 60 – $126 \text{ GeV}/c^2$ is $N_0 = 2656$. The data distribution $d\tilde{N}/dm_{jj}$ is described by a combination of background (B) and resonant W/Z

signal (S),

$$\frac{d\tilde{N}}{dm_{jj}} = N_0((1 - \tilde{f})B(m_{jj}, \tilde{b}) + \tilde{f}S(m_{jj})).$$

Here, \tilde{f} is the fraction of the signal in data and \tilde{b} is the exponential slope of the background dijet mass distribution. Functions $B(m_{jj}, \tilde{b})$ and $S(m_{jj})$ represent parametrized shapes of the dijet mass spectrum for the background and the signal. The background distribution is represented by an exponential

$$B(m_{jj}, \tilde{b}) = B_0 e^{\tilde{b}m_{jj}}$$

while the signal is represented by the double Gaussian distribution function $S(m_{jj})$ described above. The functions $B(m_{jj}, \tilde{b})$ and $S(m_{jj})$ are normalized so that the area under each, over the mass range from 60 to 126 GeV/ c^2 , is 1:

$$\int_{60}^{126} B(m_{jj}, \tilde{b}) dm_{jj} = 1,$$

$$\int_{60}^{126} S(m_{jj}) dm_{jj} = 1.$$

The prediction for the number of events in the i th mass bin is

$$\tilde{N}_i(\tilde{f}, \tilde{b}) = \int_{\text{bin } i} \frac{d\tilde{N}}{dm_{jj}} dm_{jj}.$$

The cross section for production of $W\gamma$ and $Z\gamma$ ($\sigma_{W/Z\gamma}$) can be expressed in terms of the fraction \tilde{f}

$$\tilde{\sigma}_{W/Z\gamma} = \frac{N_0 \tilde{f}}{\varepsilon_{W/Z\gamma} \mathcal{L}},$$

where \mathcal{L} is the total integrated luminosity of $90 \pm 4 \text{ pb}^{-1}$ [15], and $\varepsilon_{W/Z\gamma}$ is the combined $W/Z\gamma$ event detection acceptance = 0.023 ± 0.004 . This final acceptance is an average of $\varepsilon_{W\gamma}$ and $\varepsilon_{Z\gamma}$ quoted in Tables I and II. The errors on the final acceptance are calculated as weighted average of the errors on the individual $W\gamma$ and $Z\gamma$ acceptances.

From the LO QCD predictions for the background and signal cross sections, we would expect about 1% of the events in the fit region of the dijet invariant mass spectrum (60–126 GeV/ c^2) to originate from the hadronic decay of W/Z bosons. The fit that maximizes the likelihood function $L(\tilde{f})$ gives f of -0.05 ± 0.05 , corresponding to an unphysical negative cross section. This fit to the data is shown as the solid line in Fig. 3.

Since no signal is observed, we calculate upper limits on the $W/Z\gamma$ cross section, σ , using a Bayesian procedure. After maximizing it with respect to \tilde{b} , the likelihood function depends on the parameters σ , \mathcal{L} , and $\varepsilon_{W/Z\gamma}$. A posterior probability density is obtained by multiplying this

reduced likelihood with truncated Gaussian prior densities for \mathcal{L} and $\varepsilon_{W/Z\gamma}$, with mean and width equal to the central value and uncertainty of these parameters, respectively. The cross section is assigned a uniform prior. The posterior density is then integrated over the parameters \mathcal{L} and $\varepsilon_{W/Z\gamma}$, and the upper limit for the $W/Z\gamma$ production cross section is obtained by calculating the 95th percentile of this distribution (the value of σ such that 95% of the area under this distribution is below this value). The posterior density integrated over \mathcal{L} and $\varepsilon_{W/Z\gamma}$ as a function of σ is shown in Fig. 6. The result is $\sigma(\bar{p}p \rightarrow W\gamma) \times BR(W \rightarrow jj) + \sigma(\bar{p}p \rightarrow Z\gamma) \times BR(Z \rightarrow jj) \leq 50 \text{ pb}$ compared to a standard model expectation of 13 pb.

VII. SUMMARY

We have searched for the process $\bar{p}p \rightarrow W/Z + \gamma + X$ in which the W and Z bosons decay hadronically. The sensitivity of the search is enhanced by fitting the dijet mass spectrum from $\bar{p}p \rightarrow \text{two jets} + \gamma$ to that expected from QCD models for the background and the line shape from the $W/Z \rightarrow \text{two-jet}$ decay. The standard model prediction of the cross section for $\bar{p}p \rightarrow W/Z + \gamma$, with the W/Z bosons decaying to quark-antiquark pairs, is 13 pb. This cross section is for photons with $E_T(\gamma) > 15 \text{ GeV}$, $\Delta R(\gamma - q) > 0.4$ and for $\sqrt{\hat{s}} > M_V - 3\Gamma_V$.

The data from 90 pb^{-1} of $\bar{p}p$ interactions show no evidence of this process. By integrating the likelihood function, we get a 95% confidence level upper limit to the cross section of 50 pb. This analysis method could prove effective for measuring the $W/Z \rightarrow \text{dijet}$ mass signal in this channel from a larger statistics sample of data being collected by the CDF experiment in Tevatron run 2.

ACKNOWLEDGMENTS

We thank the Fermilab staff and the technical staffs of the participating institutions for their vital contributions. We also thank Uli Baur and Jeff Owens for valuable discussions. This work was supported by the U.S. Department of Energy and National Science Foundation; the Italian Istituto Nazionale di Fisica Nucleare; the Ministry of Education, Culture, Sports, Science and Technology of Japan; the Natural Sciences and Engineering Research Council of Canada; the National Science Council of the Republic of China; the Swiss National Science Foundation; the A.P. Sloan Foundation; the Bundesministerium fuer Bildung und Forschung, Germany; the Korean Science and Engineering Foundation and the Korean Research Foundation; the Particle Physics and Astronomy Research Council and the Royal Society, UK; the Russian Foundation for Basic Research; the Comision Interministerial de Ciencia y Tecnologia, Spain; and in part by the European Community's Human Potential Programme under Contract No. HPRN-CT-20002, Probe for New Physics.

- [1] F. Abe *et al.* (CDF Collaboration), Phys. Rev. Lett. **74**, 1936 (1995); F. Abe *et al.* (CDF Collaboration), Phys. Rev. Lett. **74**, 1941 (1995); S. Abachi *et al.* (D0 Collaboration), Phys. Rev. Lett. **75**, 1028 (1995); S. Abachi *et al.* (D0 Collaboration), Phys. Rev. Lett. **78**, 3634 (1997); B. Abbott *et al.* (D0 Collaboration), Phys. Rev. D **57**, R3817 (1998).
- [2] F. Abe *et al.*, Phys. Rev. D **57**, 67 (1998).
- [3] M. Brozovic, Ph.D. thesis, Duke University, 2002.
- [4] F. Abe *et al.*, Nucl. Instrum. Methods Phys. Res., Sect. A **271**, 387 (1988).
- [5] D. Partos, Ph.D. thesis, Brandeis University, 2001.
- [6] F. Abe *et al.*, Phys. Rev. Lett. **77**, 438 (1996).
- [7] F. Abe *et al.*, Phys. Rev. D **48**, 2998 (1993).
- [8] F. Abe *et al.*, Phys. Rev. D **45**, 1448 (1992).
- [9] U. Baur and D. Zeppenfeld, Nucl. Phys. **B308**, 127 (1988); U. Baur and E. L. Berger, Phys. Rev. D **47**, 4889 (1993).
- [10] G. Marchesini *et al.*, Comput. Phys. Commun. **67**, 465 (1992).
- [11] H. Baer, J. Ohnemus, and J. F. Owens, Phys. Rev. D **42**, 61 (1990).
- [12] T. Sjöstrand, Comput. Phys. Commun. **82**, 74 (1994).
- [13] U. Baur (private communication).
- [14] F. Abe *et al.*, Phys. Rev. D **41**, 1722 (1990).
- [15] D. Cronin-Hennesy, A. Beretvas, and F. Derwent, Nucl. Instrum. Methods Phys. Res., Sect. A **443**, 37 (2000).